Available online at www.sciencedirect.com
SCIENCE DIRECT®
International Journal of Heat and Mass Transfer 47 (2004) 2901–2912
International Journal of HEAT and MASS TRANSFER
www.elsevier.com/locate/ijhmt

A numerical study of thermo-fluid phenomena in metal hydride beds in the hydriding process

Man Yeong Ha [a,*], In Kyu Kim [b], Ha Doo Song [a], Sikyong Sung [b], Dong Hyuk Lee [b]

[a] School of Mechanical Engineering, Pusan National University San 30, Chang Jeon Dong, Kum Jeong Gu, Pusan 609-735, South Korea
[b] Research Laboratory, LG Electronics, 391-2, Gaeumjeong-dong, Chanwon City, Gyeongnam 641-711, South Korea

Received 12 November 2003; received in revised form 19 March 2004

Abstract

Two-dimensional solution for unsteady heat and mass transfer in metal hydride bed in the hydriding process is obtained using a finite volume method in order to understand the physical mechanisms occurring in the bed. We considered the effects of different thermal conductivities, bed diameters and the presence of fins on thermo-fluid phenomena occurring in the bed. The present results show that the whole process occurring in the bed is governed and controlled by heat transfer from the bed to the surrounding cooling fluid. So we need to develop the method to improve and enhance the heat transfer rate from the bed to the surrounding cooling fluid in order to apply the metal hydride bed to the heat exchanging system efficiently. The higher thermal conductivity, smaller bed diameter and the presence of fins in the bed give more enhanced heat transfer rate from the bed. The present computational results are compared with the experimental data to check the validity of the present calculation, showing the good agreement between them.

1. Introduction

The hydrogen is being focused as the energy source, which will replace the current fossil fuel and be used in the wide application range at the 21st century. In using such hydrogen, the metal hydride is considered as the new alternative material now. The metal hydride has the absolute hydrogen quantity which can bear at the metal temperature condition and has the property of the chemical reaction which can absorb or desorb the hydrogen according to the mutual relations with the surrounding hydrogen pressure. Also the metal hydride accompanies the thermal flow, which puts out the generated heat or absorbs the surrounding heat in the reaction process. Thus, if we can apply the metal hydride to the heat exchanger or the heat pump, the metal hydride can succeed as the new alternative material, which can overcome the various limits experienced in the system using the existing heat-exchanging material. However, there exist some problems to apply the metal hydride to the real applications, because we consider various chemical parameters involved in the hydrogen reaction occurring in the porous media of metal hydride bed. It is difficult to predict accurately the physical phenomena occurring in the bed only by using the experimental approaching method. The size of metal hydride particles is normally about dozens micron, making the experimental approaches difficult for the correct prediction of physical phenomena in the bed. Thus the numerical approaching method is necessary to make up for the weak points of experimental study and to understand fully the hydrogen reaction and heat transfer mechanisms in the bed for the design of efficient heat exchanger.

Many researchers have carried out studies to understand the physical mechanisms occurring in the metal hydride bed and to find out the methods to control the

* Corresponding author. Tel.: +82-51-510-2440; fax: +82-51-512-9835.
E-mail address: myha@pusan.ac.kr (M.Y. Ha).

0017-9310/$ - see front matter © 2004 Elsevier Ltd. All rights reserved.
doi:10.1016/j.ijheatmasstransfer.2004.03.014

Nomenclature

a_p	effective surface area (m^2)
C_p	specific heat (J/kg K)
E	activation energy (J/mol)
F	reacted fraction
h_p	heat transfer coefficient between gas and solid (W/m^2 K)
K	permeability (m^2)
$\dot{m}$	hydrogen mass absorbed or desorbed (kg/m^3 s)
M	molecular weight (kg/mol)
P	pressure (Pa)
$\dot{Q}$	volumetric heat generation rate (J/m^3)
R	universal gas constant ($J/mol\,K^{-1}$)
T	temperature (K)
t	time (s)
V	gas velocity (m/s)

Greek symbols

ΔH	reacted heat (J/kg)
ε	porosity
λ	thermal conductivity ($W/m\,K^{-1}$)
η	dynamic viscosity (kg/m s)
ρ	density (kg/m^3)

Subscripts

a	absorption
Al	aluminum
b	bulk
d	desorption
eff	effective
eq	equilibrium
g	gas
ge	gas effective
s	solid
se	solid effective
ss	saturated
o	initial

hydrogen reaction for a long time. Inomata et al. [1] measured and modeled the hydriding and dehydriding kinetics to show what is the rate controlling process in the hydriding and dehydriding rates. Ben Nasarallah and Jemni [2] carried out the numerical analysis for the thermo-fluid phenomena in the two-dimensional porous media using some hypotheses and verified their hypotheses by comparing the results with and without these hypotheses. Nakagawa et al. [3] predicted the transient heat and mass transfer phenomena in the porous media of metal hydride bed using a two-dimensional mathematical model with hydriding and dehydriding kinetics. Jemni et al. [4] carried out an experimental study to determine the equilibrium pressure, the reaction kinetics, effective thermal conductivity, heat and mass transfer in the $LaNi_5$-H_2 system. They also developed the theoretical model and checked its validity by comparison with the experimental results of temperature and pressure evolution in the bed. Aldas et al. [5] carried out the time-dependent and three-dimensional numerical analysis to investigate heat and mass transfer, fluid flow and chemical reaction in the bed using the general-purpose commercial code. The effects of the presence of fins on the performance of metal hydride bed were investigated by Kim et al. [6] and Guo and Sung [7] by predicting the conjugate heat and mass transfer analysis in the bed.

The metal hydride bed generates heat when the metal hydride absorbs hydrogen. This reaction can be maintained under the condition that the equilibrium and surrounding gas pressure sustain their difference. However, if the reacted fraction increases during the absorption process, the equilibrium pressure approaches rapidly to the surrounding gas pressure and the first reaction in the bed stops. Therefore, we should maintain the pressure difference for the continuous second reaction in the bed. In order to maintain this pressure difference in the bed, we should transfer the heat generated in the porous bed very quickly and efficiently to the surrounding cooling environment. However, most of metal hydrides have low thermal conductivity, which is generally less than 1. The thermal diffusion process in the bed is much slower than the fast reaction process and the total process occurring in the bed is governed by the thermal diffusion. Thus we should develop the method to enhance the heat transfer rate in the bed in order to apply the metal hydride bed to the thermal system efficiently. In order to understand the physical mechanism for the reaction, heat and mass transfer in the bed and to obtain the conditions to control the heat flow in the bed effectively, we carried out the numerical simulation to solve the governing equations for mass, momentum and energy conservation with chemical reaction. We considered the effects of different thermo-physical properties, bed diameters and the presence of fins on the thermo-fluid phenomena occurring in the metal hybrid bed. The computational results are compared with experimental data [8] to check the validity of the present calculation and represent well the measured data.

2. Mathematical models

Fig. 1 shows a schematic diagram for the bed packed with particle powders of metal hydrides whose particle diameter is 50 μm. The four different cases considered in

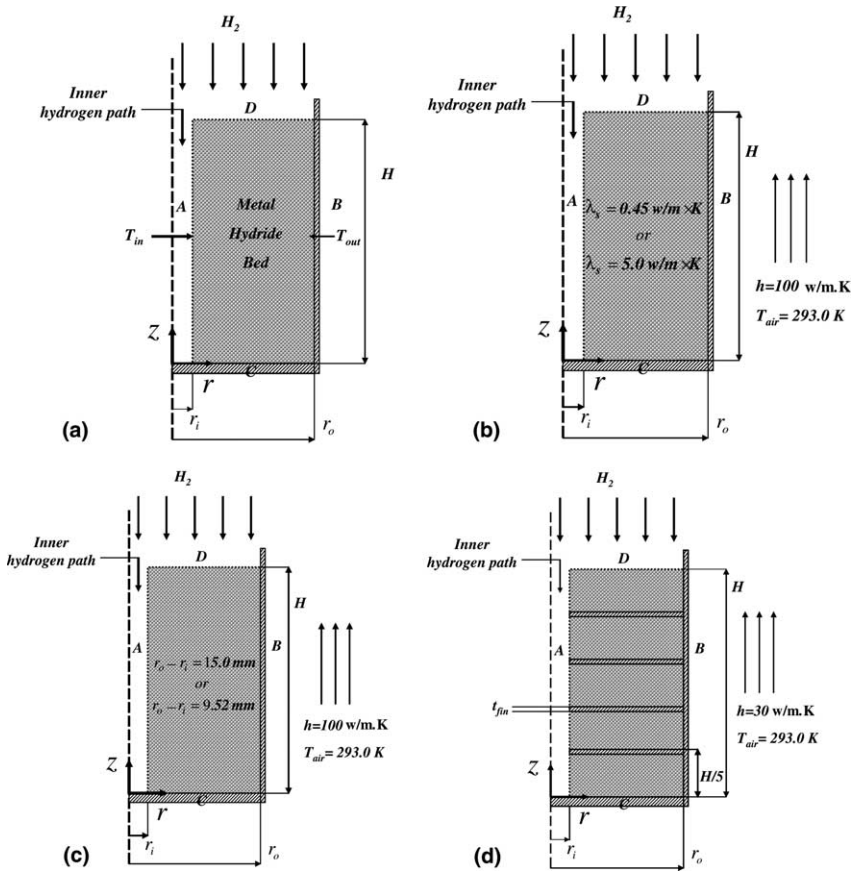

Fig. 1. A schematic diagram for different cases considered in the present study.

the present study are also shown in this figure. In order to investigate the physical phenomena occurring in the bed shown in Fig. 1, we solve the following governing equations [1–7]. The continuity equation in this porous media of metal hydride bed is defined as

$$\frac{\partial(\varepsilon\rho_{\mathrm{g}})}{\partial t}+\nabla\cdot(\rho_{\mathrm{g}}\boldsymbol{u})=-\dot{m} \tag{1}$$

where ε, ρ, $\boldsymbol{u}$, t and $\dot{m}$ represent the porosity, density, velocity, time and hydrogen mass absorbed due to reaction. The subscript g in Eq. (1) represents the gas phase. The Darcy's law is used to calculate the gas velocity in the porous media.

$$\boldsymbol{u}=-\frac{K}{\eta_{\mathrm{g}}}\nabla P \tag{2}$$

where K, η and P represent the permeability, dynamic viscosity and pressure, respectively. The ideal gas law is used by assuming the hydrogen as an ideal gas.

$$P=\frac{\rho_{\mathrm{g}}RT}{M_{\mathrm{g}}} \tag{3}$$

where R, T and M_{g} represent the universal gas constant, temperature and molecular weight of hydrogen, respectively. Substituting $\boldsymbol{u}$ from Eq. (2) and P from Eq. (3) into Eq. (1), we can derive the following equation to solve the gas phase pressure:

$$\frac{\partial}{\partial t}\left(\frac{\varepsilon M_{\mathrm{g}}}{RT}P\right)-\nabla\cdot\left[\frac{M_{\mathrm{g}}P}{RT}\left(\frac{K}{\eta_{\mathrm{g}}}\right)\nabla P\right]=-\dot{m} \tag{4}$$

When we use the assumption of local temperature equilibrium under which the temperature difference between the metal and the surrounding gas can be neglected, the energy equation is defined as

$$\rho_{\mathrm{b}}c_{\mathrm{pb}}\frac{\partial T}{\partial t}+\nabla\cdot(\rho_{\mathrm{g}}c_{\mathrm{pg}}\boldsymbol{u}T)=\nabla\cdot(\lambda_{\mathrm{eff}}\nabla T)+(1-\varepsilon)\dot{Q} \tag{5}$$

where

$$\rho_{\mathrm{b}}c_{\mathrm{pb}}=\varepsilon\rho_{\mathrm{g}}c_{\mathrm{pg}}+(1-\varepsilon)\rho_{\mathrm{s}}c_{\mathrm{ps}},\quad \lambda_{\mathrm{eff}}=\lambda_{\mathrm{se}}+\varepsilon\lambda_{\mathrm{g}} \tag{6}$$

Here c, λ and $\dot{Q}$ are the specific heat, thermal conductivity and volumetric heat generation rate due to reaction. The subscript s in these equations represents the solid phase. If the fins are present in the bed, we should

solve simultaneously the following conduction equation to govern the temperature distribution in the fins.

$$(\rho C_p)_{fin}\frac{\partial T_{fin}}{\partial t} = \nabla(k_{fin}\nabla T_{fin}) \tag{7}$$

In order to solve and close all these governing equations, we need some auxiliary equations to define the thermo-physical properties and reaction rate as a function of porosity, temperature, pressure, etc. The hydrogen mass, $\dot{m}$, absorbed due to hydriding reaction in Eq. (1) is expressed as

$$\dot{m} = C_a \exp\left(-\frac{E_a}{RT}\right)\ln\left(\frac{P_g}{P_{eq}}\right)(\rho_{ss}-\rho_s) \tag{8}$$

where P_{eq}, ρ_{ss}, E_a and C_a represent the plateau pressure at the equilibrium state, density of metal hydride at the saturation state, activation energy and material constant during the absorption process. The permeability used in Eq. (2) to obtain the hydrogen velocity is defined as

$$K = K_D(1+\zeta K_n) \tag{9}$$

where,

$$K_D = \frac{d_p^2\varepsilon^3}{180(1-\varepsilon)^2}, \quad K_n = \frac{l_g}{L_c}, \quad L_c = K_D^{1/2},$$
$$l_g = \frac{\eta_g}{P}\left(\frac{\pi RT}{2M_g}\right)^{1/2}, \quad \zeta = 1.15 \tag{10}$$

Here d_p represents the diameter of metal hydride. The effective thermal conductivity for the metal hydride used in Eq. (6) is defined as

$$\lambda_{se} = 0.45 + \varepsilon\lambda_g \tag{11}$$

The size of the metal hydride changes during the reaction process as a function of the particle reacted fraction F as follows:

$$d_p = d_{po}(1+\alpha F)^{1/3} \tag{12}$$

where d_{po} and α represent the initial particle diameter and the coefficient of volume expansion whose value is 0.243. The density of the metal hydride particle also depends on the particle fraction defined as

$$\rho_s = \rho_{so}\frac{(1+WT\cdot F)}{1+\alpha F} \tag{13}$$

where ρ_{so} and WT are the initial particle density and maximum hydrogen to metal atomic ratio absorbed, respectively.

The hydriding reaction rate used in this study is derived by assuming that the hydrogen absorption occurs through a series of nucleation, growth and diffusion process through the hydrogen layer and is defined as

$$\frac{dF}{dt} = \frac{1}{1/k_1 + 1/k_2} \tag{14}$$

where

$$k_1 = 0.216(P-P_{eq})(1-F)[-\ln(1-F)]^{2/3},$$
$$k_2 = \frac{4\pi RD(P-P_{eq})}{(1-F)^{-1/3}-1} \tag{15}$$

where $4\pi RD = 5.278\times10^{-3}$. Here k_1 shows the equation to represent the nucleation and growth rate as a function of pressure difference from the equilibrium pressure and reaction fraction, whereas k_2 represents the diffusion rate through the hydride layers. The equilibrium pressure, P_{eq}, for absorption is defined as

$$P_{eq} = \exp[(11.371 - 2927.7/T_g) + \psi\times|\tan(\pi(F-0.5))|^{1.5} \times \mathrm{sign}(\tan(\pi(F-0.5)))] \tag{16}$$

where

$$\psi = 0.2324\times\exp(-0.0026\times(T_g-273.15))$$
$$\mathrm{sign}(\tan(\pi(F-0.5))) = 1 \quad \text{if } \tan(\pi(F-0.5)) \geqslant 0$$
$$\mathrm{sign}(\tan(\pi(F-0.5))) = -1 \quad \text{if } \tan(\pi(F-0.5)) < 0 \tag{17}$$

Table 1 shows thermo-physical properties and geometrical dimension for different cases shown in Fig. 1. Case 1 simulates the experimental case carried out by the present authors. All thermo-physical properties for the Case 1 in Table 1 are obtained by the experiment [8]. The temperature results obtained by the present calculation are compared with the experimental data to validate the present numerical computation. Cases 2, 3 and 4 consider the effects of thermal conductivity, bed diameter and fin presence on thermo-fluid phenomena occurring in the bed. Tables 2 and 3 show the initial and boundary conditions used for Eqs. (4) and (5) for pressure and temperature. T_{in} and T_{out} in Table 3 represent the measured temperature values at the center ($r=0$) and outer wall ($r=R$) of bed.

The governing equations with initial and boundary conditions given in Tables 2 and 3 are solved numerically using the finite volume method [9]. This approach allows for treatment of arbitrary geometries and avoids problems with metric singularities usually associated with a finite difference method. To initiate, we first integrate the differential conservation equations over a finite volume V enclosed by surface S. The volume integral for the flux vector is converted to a surface integral through the Gauss divergence theorem. The resulting integral conservation equation is discretized by using a hybrid-difference scheme for convection terms and a central-difference scheme for diffusion terms. The bed packed with particle powders of metal hydrides and fin regions are solved simultaneously by introducing a block parameter, which distinguish a fin region from a

Table 1
Thermo-physical properties of materials and data used in the present computation

Case	Case 1	Case 2	Case 3	Case 4
Parameter	Code validation	Thermal conductivity variation	Bed diameter variation	Fin effect
$(r_o - r_i)$ (mm)	19.12	19.12	15.0	19.12
	9.52		H (mm)	270.0
270.0	130.0	270.0	α	0.243
0.243	0.243	0.243		0.004
	λ_S (W/m K)	0.45	0.45	0.45
0.45		5.00		C_p (J/kg K)
400.0	400.0	400.0	400.0	
479.0		ε	0.428	0.428
0.428	0.428		0.140	
Wt (%)	1.1	1.1	1.1	1.1
Fin	w/o	w/o	w/o	w/
Fin thickness (mm)	w/o	w/o	w/o	0.1

w/o: case without fin, w/: case with fin.

Table 2
Initial conditions used in the present computation

Parameters	Value
P_g (Pa)	0.36×atm
T_g (K)	274.6
Initial fraction	0.08

bed region, into discretized governing equations. Thus convection terms are automatically turned off in the fin region, and energy balance in the bed-fin interface is carefully set up to make sure that the matching conditions of continuous temperature and heat flux at the interface are satisfied.

3. Results and discussion

The reaction in the bed is proportional to the absolute pressure difference between the gas pressure and the equilibrium pressure $(P_g - P_{eq})$. In the case that the gas pressure is constant, the reaction becomes more active as the temperature in the bed and the corresponding equilibrium pressure becomes lower. In other case that the temperature in the bed and the corresponding equilibrium pressure are constant, the reaction becomes more active with increasing gas pressure. Fig. 2 shows the schematic diagram for this reaction mechanism in the bed. Fig. 3 shows the reaction process as a function of the gas pressure, equilibrium pressure, reacted fraction and temperature. Figs. 4–7 show the contours for

Table 3
Boundary conditions used in the present computation

Case	Face	A	B	C	D
Case 1	P_g	$\frac{\partial P(0,z)}{\partial r} = 0$	$\frac{\partial P(R,z)}{\partial r} = 0$	$\frac{\partial P(r,0)}{\partial z} = 0$	$p_g(r,H) = P_{go}$
	T_g	$T(0,z) = T_{in}$	$T(R,z) = T_{out}$	$\frac{\partial T(r,0)}{\partial z} = 0$	$-k_{eff}\frac{\partial T(r,H)}{\partial r} = \rho_g C_{pg}\langle V\rangle(T_0 - T)$
Case 2 and Case 3	P_g	$\frac{\partial P(0,z)}{\partial r} = 0$	$\frac{\partial P(R,z)}{\partial r} = 0$	$\frac{\partial P(r,0)}{\partial z} = 0$	$p_g(r,H) = P_{go}$
	T_g	$\frac{\partial T(0,z)}{\partial r} = 0$	$h = 100$ W/m^2 K	$\frac{\partial T(r,0)}{\partial z} = 0$	$-k_{eff}\frac{\partial T(r,H)}{\partial r} = \rho_g C_{pg}\langle V\rangle(T_0 - T)$
Case 4	P_g	$\frac{\partial P(0,z)}{\partial r} = 0$	$\frac{\partial P(R,z)}{\partial r} = 0$	$\frac{\partial P(r,0)}{\partial z} = 0$	$p_g(r,H) = P_{go}$
	T_g	$\frac{\partial T(0,z)}{\partial r} = 0$	$h = 30$ W/m^2 K	$\frac{\partial T(r,0)}{\partial z} = 0$	$-k_{eff}\frac{\partial T(r,H)}{\partial r} = \rho_g C_{pg}\langle V\rangle(T_0 - T)$

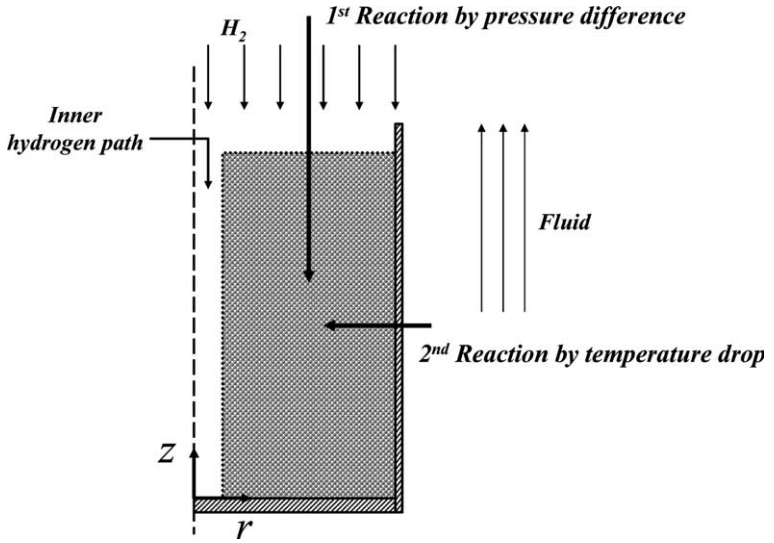

Fig. 2. A schematic diagram to show the reaction mechanism in the bed.

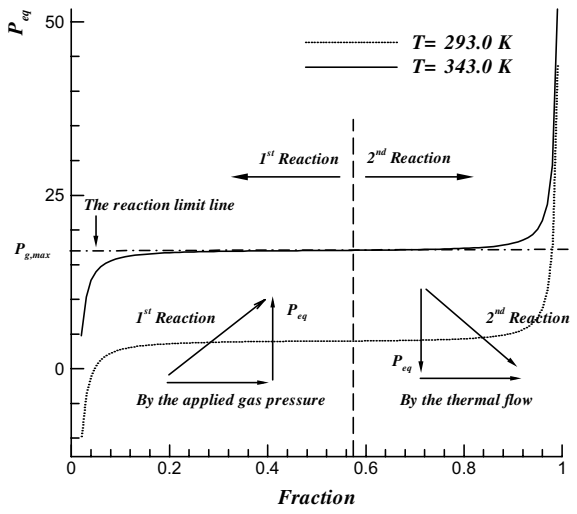

Fig. 3. The reaction process as a function of the gas pressure, equilibrium pressure, reacted fraction and temperature.

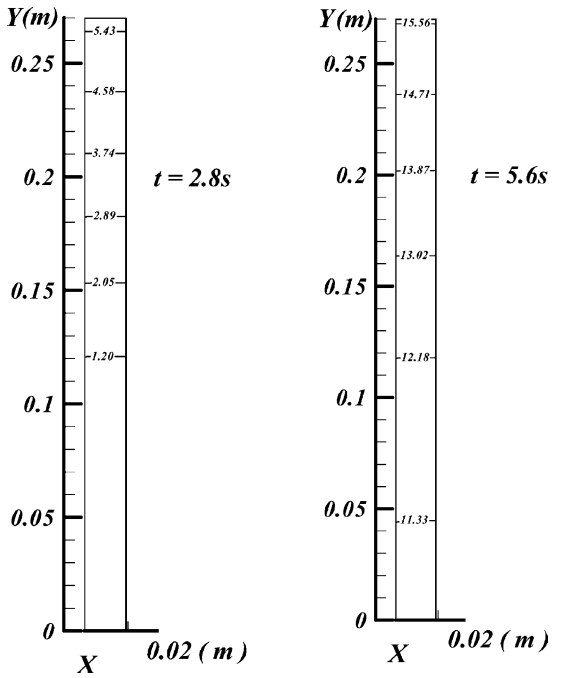

Fig. 4. Contours of gas pressure in the bed as a function of time.

the gas pressure, equilibrium pressure, reacted fraction and temperature in the bed as a function of time. Fraction increases by the applied pressure in the first reaction. Because the initial temperature in the bed has a constant value of 293 K, the first reaction in the bed occurs mainly due to the pressure difference between the equilibrium pressure corresponding to the initial temperature in the bed and the gas pressure applied at the top of bed ($z = H$). The temperature and the corresponding equilibrium (plateau) pressure in the bed increase very rapidly due to heat generation during the first reaction. If the temperature approaches to the maximum value around a value of 343 K and the corresponding equilibrium pressure is close to the applied gas pressure, the pressure difference, $P_g - P_{eq}$, becomes very small and the first reaction due to this pressure difference almost stops at the entire domain of bed. After the first reaction stops and the gas pressure in the bed has an almost constant value close to the applied gas

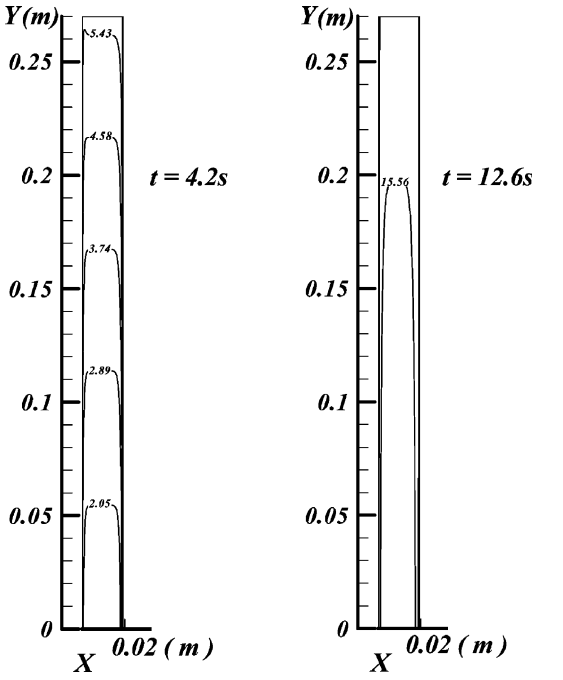

Fig. 5. Contours of equilibrium pressure in the bed as a function of time.

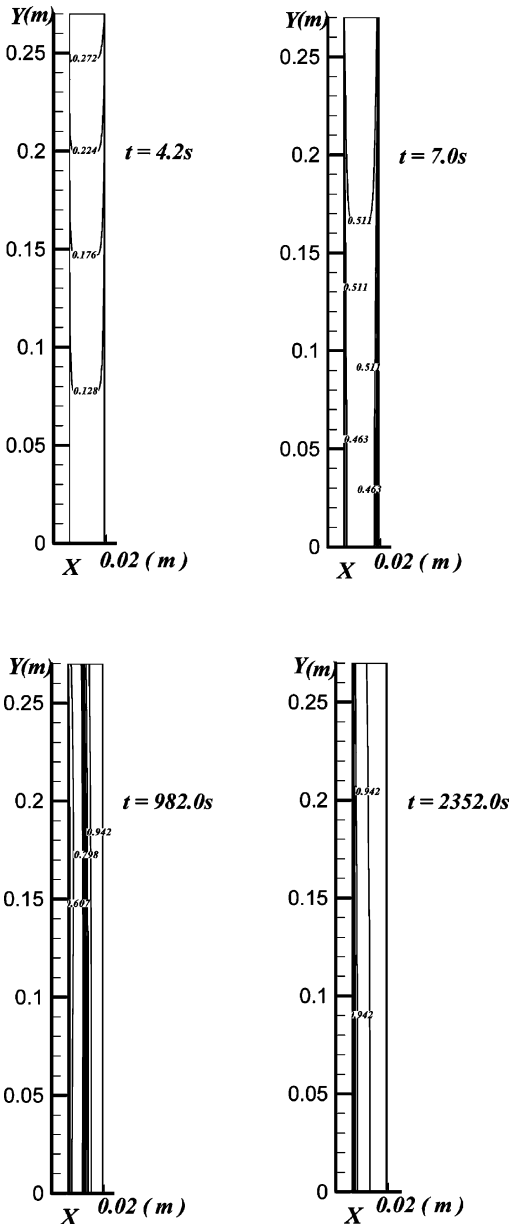

Fig. 6. Contours of reacted fraction in the bed as a function of time.

pressure, the second reaction starts to work with heat transfer from the hot bed to the surrounding cold air. If the temperature in the bed decreases due to heat transfer to the surrounding cold air, the corresponding equilibrium pressure decreases, forming the pressure difference, $P_g - P_{eq}$, for the second reaction.

Fig. 8 shows the reacted fraction velocity, dF/dt in Eq. (14), for the Case 1 shown in Fig. 1 and Table 1. This figure shows the reacted fraction velocity at different radial positions of $r = 5$, 8, 11.5, 15 and 18 mm and at the center ($z = 135$ mm) in the axial direction. At the initial stage of first reaction, the applied gas pressure is higher than the initial plateau pressure of the bed as mentioned above, resulting in the explosive hydrogen absorption and rapidly increasing reaction rate in the bed. At the end of the first reaction, the equilibrium (plateau) pressure approaches to the applied gas pressure, the temperature has a maximum value and the first reaction stops in the almost entire domain of bed. After the temperature of bed reaches the maximum value, the temperature and corresponding equilibrium pressure start to decrease from the outside of the bed owing to heat transfer from the bed to the cooling air. Thus the pressure difference, $P_g - P_{eq}$, is formed in the bed again and the second reaction starts to work from the outside of bed. At the outside of bed ($r = 18$ mm) the reacted fraction velocity and reacted fraction increase during the first period of second reaction with increasing pressure difference formed in the bed. If the reacted fraction is greater than a certain critical value, the equilibrium pressure increases again even though the temperature keeps decreasing due to heat transfer, as shown in Fig. 3. As a result, during the second period of second reaction, the pressure difference and reacted fraction velocity keep decreasing until the second reaction stops at $r = 18$ mm. The second reaction started at $r = 18$ mm is propagated into the inward direction sequentially, as shown in Fig. 8. The shape of reacted fraction velocity at $r = 5$, 8, 11.5 and 15 mm is generally similar to that at $r = 18$ mm. The

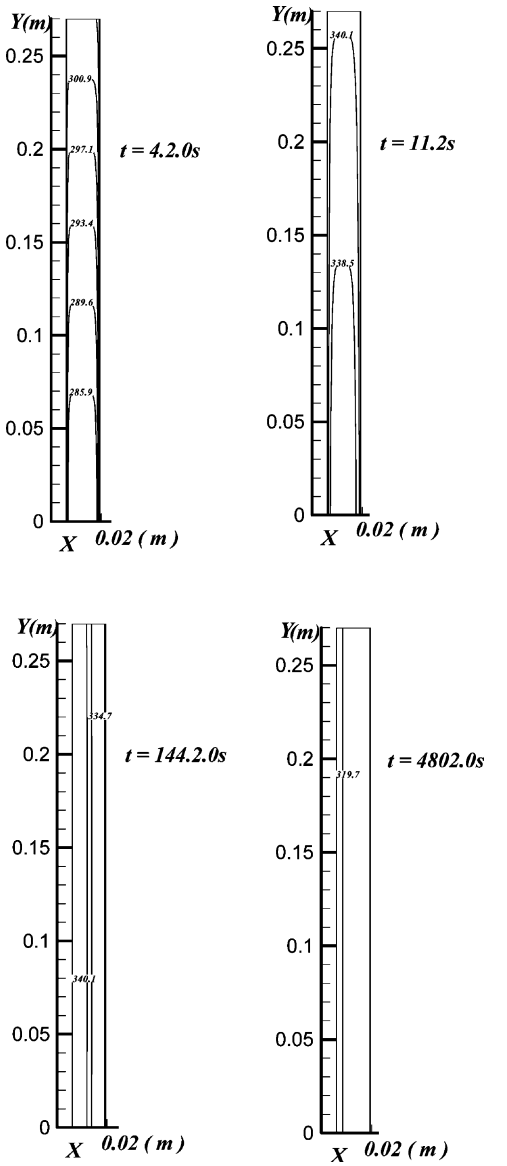

Fig. 7. Contours of temperature in the bed as a function of time.

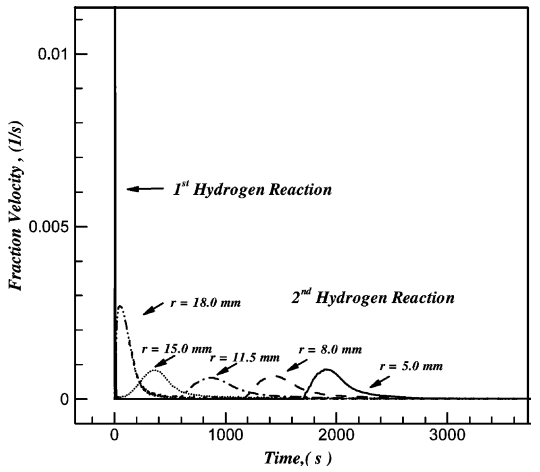

Fig. 8. Time history of reacted fraction velocity at different radial positions for the Case 1.

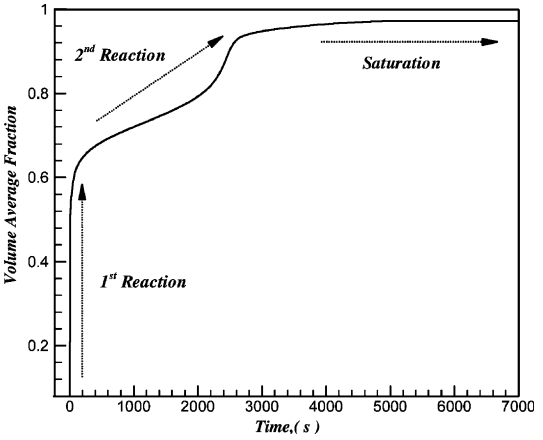

Fig. 9. Time history of volume-averaged reacted fraction in the bed for the Case 1.

time required for the first reaction is negligibly small compared to that for the second reaction. The whole process occurring in the bed during the second reaction is governed and controlled by the thermal diffusion process, because the time required for heat transfer is much greater than that for chemical. Thus this result shows it is very important to control the thermal diffusion process effectively in order to design the efficient thermal system using the metal hydride bed.

Fig. 9 shows the volume-averaged reacted fraction in the bed as a function of time for the Case 1. During the first reaction with the initial explosive reaction, the volume-averaged reacted fraction increases very steeply. The increasing rate of volume-averaged reacted fraction during the second reaction is slower than that during the first reaction, because the temperature in the bed decreases slowly due to slow heat transfer from the bed to the surrounding cooling air. After $t = 2600$ s, the volume-averaged reacted fraction increases very slowly and approaches the saturation sate because the temperature in the bed approaches the surrounding cooling air temperature.

Fig. 10 shows the time history of temperature at different radial positions of $r = 5$, 8, 11.5, 15, 18 mm and at the center in the axial direction for the Case 1. For the reasons mentioned above, the temperatures at $r = 5$, 8, 11.5, 15 and 18 mm increase very rapidly due to explosive reaction occurring in the entire domain of bed

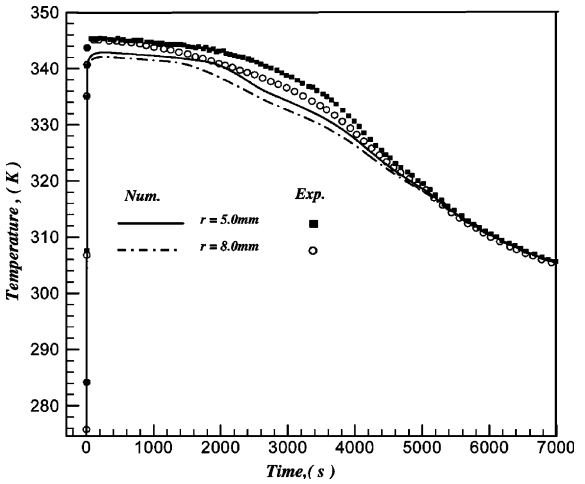

Fig. 10. Time history of temperature at different radial positions for the Case 1.

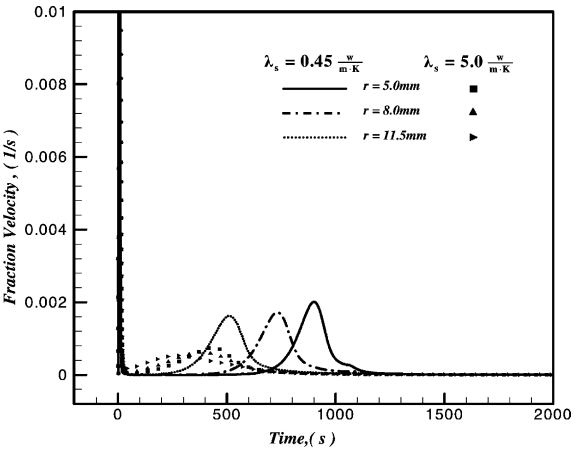

Fig. 11. Time history of reacted fraction velocity at different radial positions for the Case 2 with different thermal conductivities of $\lambda_S = 0.45$ and 5.0 W/m K.

during the first reaction period, giving almost same temperature history at different radial positions. During the second reaction period, the temperature in the bed decreases due to heat transfer from the bed to the surrounding cooling air. If the heat transfer in the bed occurs in a pure conduction mode without any heat generation during second reaction period, the temperature in the bed decreases more quickly and approaches to the surrounding cooling air temperature more rapidly than the present case with heat generation due to reaction. We compared the present computational results with the experimental data [8] to check the validity of the present calculation results and mathematical model. The present computational results represent well the experimental data as shown in Fig. 10. Especially, even though the temperatures in the bed increase very rapidly during the first reaction period, the present calculation results agree well with measured data.

Fig. 11 shows the time history of fraction velocity at different positions of $r = 5$, 8 and 11.5 mm for the Case 2 in Fig. 1 and Table 1 to consider the effect of different thermal conductivities of $\lambda_S = 0.45$ and 5.0 W/m K on heat transfer and reaction in the bed. The lines and symbols represent the results for $\lambda_S = 0.45$ and 5.0 W/m K, respectively. Fig. 12 shows the volume-averaged reacted fraction as a function of time for Case 2 with different thermal conductivities. The first reaction occurs very rapidly for both cases of high and low thermal conductivities. The time required for the first reaction is almost the same for both cases. The value of volume-averaged reacted fraction at the end of first reaction for $\lambda_S = 5.0$ W/m K is higher than that for $\lambda_S = 0.45$ W/m K, because the temperature and corresponding reaction rate increase owing to increasing heat transfer with increasing thermal conductivity. However, we can observe big differences in reacted fraction velocity, volume-

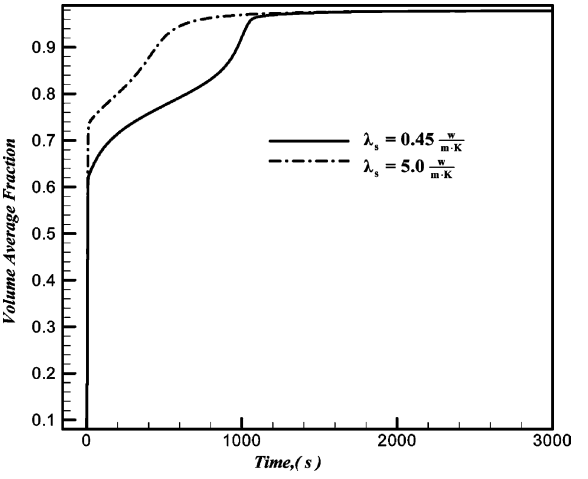

Fig. 12. Time history of volume-averaged reacted fraction for the Case 2 with different thermal conductivities of $\lambda_S = 0.45$ and 5.0 W/m K.

averaged reacted fraction and temperature during the second reaction for different thermal conductivities. For the case of lower thermal conductivity of $\lambda_S = 0.45$ W/m K, the second reaction starts from the outside of bed and is propagated sequentially into the inward direction, similar to the Case 1. However, because the heat transfer rate from the bed to the cooling environment increases when we increase the thermal conductivity to $\lambda_S = 5$ W/m K, the temperature in the bed decrease more quickly and the second reaction occurs almost simultaneously at all positions, resulting in the small differences in time to start and end the second reaction at different positions of $r = 5$, 8 and 11.5 mm, compared to the case of lower thermal conductivity. Thus the volume-averaged reacted

fraction for $\lambda_S = 5.0$ W/m K approaches more quickly to the saturation value than $\lambda_S = 0.45$ W/m K during the second reaction.

Fig. 13 shows the time history of temperature at the position of $r = 5$ mm for the Case 2 with different thermal conductivities of $\lambda_S = 0.45$ and 5.0 W/m K. The temperature increases very rapidly during the first explosive reaction. The temperature history for $\lambda_S = 5.0$ W/m K during the first reaction period is almost the same as that for $\lambda_S = 0.45$ W/m K. However, during the second reaction period, the temperature for $\lambda_S = 5.0$ W/m K decreases more quickly than that for $\lambda_S = 0.45$ W/m K owing to increasing heat transfer from the bed to the cooling environment with increasing thermal conductivity.

Figs. 14 and 15 show the time history of reacted fraction velocity and temperature, respectively, at different positions of $r = 0.26$, 0.42 and $0.6d_0$ for the Case 3 in Fig. 1 and Table 1 with different bed diameters of $d_0 = 9.52$ and 15 mm. The symbols and lines represent the results for $d_0 = 9.52$ and 15 mm, respectively. Fig. 16 shows the volume-averaged reacted fraction as a function of time for the Case 3 with different bed diameters. The pattern of reaction is generally similar to the previous cases with the explosively rapid first reaction, which is followed by the second reactions starting from the outside and propagating into the inside sequentially. With decreasing bed diameter, the temperature in the bed decreases more rapidly during the second reaction. Thus the second reactions occurring at different radial positions for the case of smaller bed diameter start and finish their reaction process at much earlier time than that for larger bed diameter. The reacted fraction for smaller bed diameter also reaches the saturation state more quickly than that for the larger bed diameter.

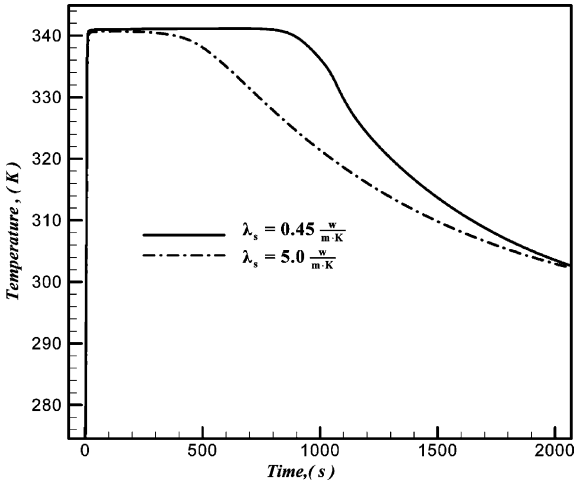

Fig. 13. Time history of temperature at the position of $r = 5$ mm for the Case 2 with different thermal conductivities of $\lambda_S = 0.45$ and 5.0 W/m K.

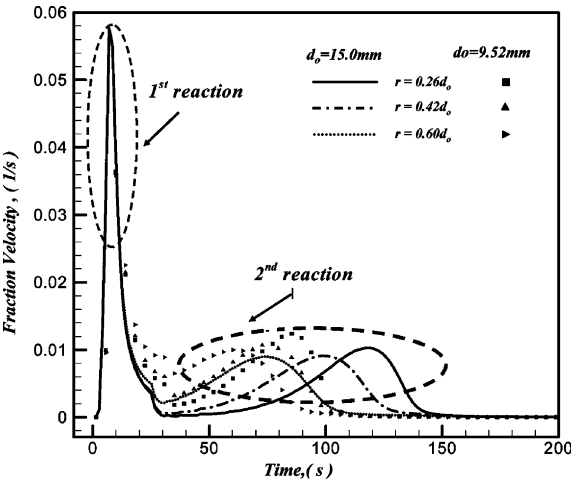

Fig. 14. Time history of reacted fraction velocity at different radial positions for the Case 3 with different bed diameters of $d_0 = 9.52$ and 15 mm.

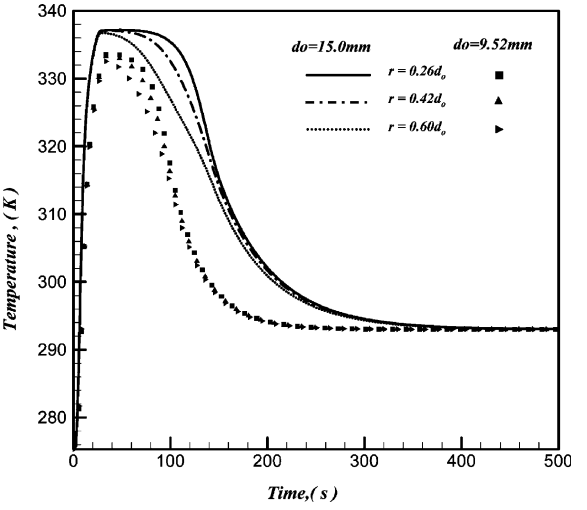

Fig. 15. Time history of temperature at different radial positions with different bed diameters of $d_0 = 9.52$ and 15 mm.

In order to see the effects of the presence of fins on heat transfer and reaction in the bed, we inserted the radial fins in the bed corresponding to the Case 4 shown in Fig. 1 and Table 1. The results with fins are compared with those without fins. Figs. 17 and 18 show the time history of fraction velocity and temperature at different radial positions of $r = 5$ and 15 mm for different cases with and without fins. The lines and symbols represent the results for the cases with and without fins, respectively. Fig. 19 shows the volume-averaged reacted fraction as a function of time for different cases with and without fins. Because the first reaction occurs explosively for both cases with and without fins, the time history for

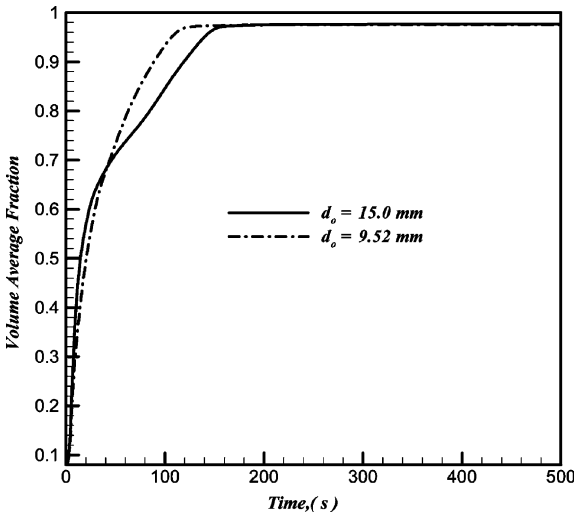

Fig. 16. Time history of volume-averaged reacted fraction for the Case 3 with different bed diameters of $d_0 = 9.52$ and 15 mm.

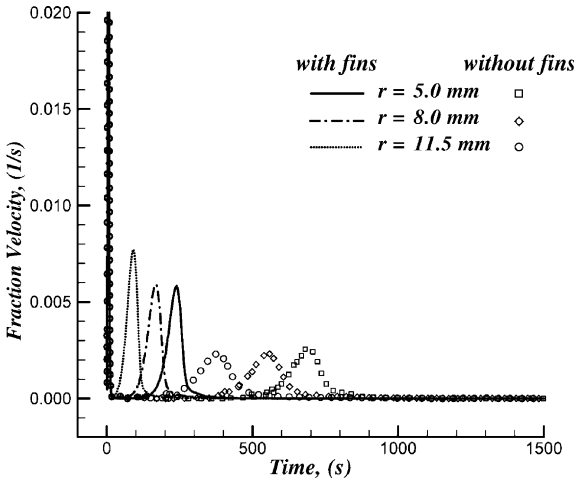

Fig. 17. Time history of reacted fraction velocity at different radial positions of $r = 5$, 8 and 11.5, 15 mm for the Case 4 with and without fins.

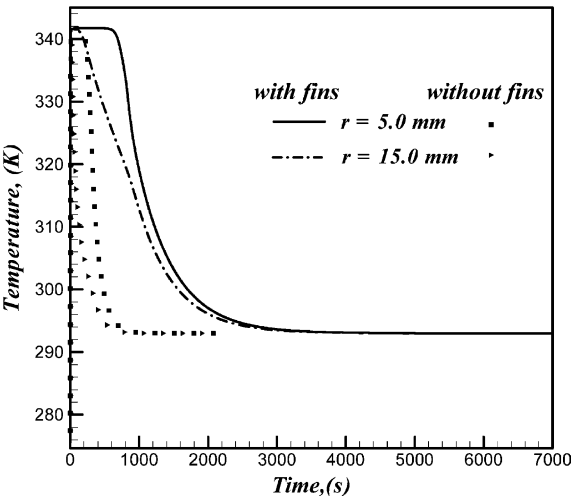

Fig. 18. Time history of temperature at different radial positions of $r = 5$ and 15 mm for the Case 4 with and without fins.

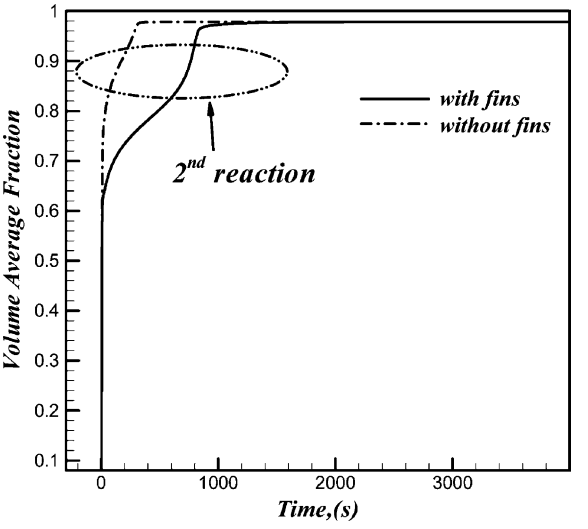

Fig. 19. Time history of volume-averaged reacted fraction for the Case 4 with and without fins.

reacted fraction velocity, temperature and volume-averaged reacted fraction for the case with fins is almost the same as that without fins. However, the second reaction process is controlled by the heat transfer rate from the bed to the cooling fluid. In the presence of fins, the heat transfer rate increases owing to the increase in both heat transfer area and thermal conductivity. The fins used are aluminum, whose thermal conductivity is 237 W/m K. The thermal conductivity of fins is much larger than the thermal conductivity of bed, whose value is 0.45 W/m K. Thus the temperature for the case with fins decreases much faster and approaches to the cooling fluid temperature more quickly than that without fins. The second reactions at different positions for the case with fins start and finish their process at much earlier time than those without fins. The volume-averaged reacted fraction for the case with fins also approaches to the saturation state more quickly than that without fins.

4. Conclusions

We investigated the thermo-physical phenomena occurring in the metal hydride bed by solving numerically

the unsteady, two-dimensional mass, momentum and energy conservation equations with chemical reactions in order to understand the physical mechanisms occurring in the metal hydride bed. The first hydrogen reaction in the bed occurs very rapidly owing to the big pressure difference caused by the applied gas pressure, resulting in the very fast increase in temperature and corresponding equilibrium pressure in the bed. However, the second reaction occurs very slowly owing to slow heat transfer from the bed to the surrounding cooling fluid with low thermal conductivity of the metal hydride particles, resulting in the slow decrease in temperature and equilibrium pressure. Thus the total process in the metal hydride bed is governed and controlled by the heat transfer in the bed. In order to decrease the total process time required for the hydriding reaction by increasing the heat and mass transfer in the bed, we should increase thermal conductivity of metal hydride particles, decrease bed diameter and insert fins in the bed.

Acknowledgements

This work was partially supported by the LG Electronics, BK21 and NRL projects.

References

[1] A. Inomata, H. Aoki, T. Miura, Measurement and modeling of hydriding and dehydriding kinetics, J. Alloy Compd. 278 (1998) 103–109.
[2] S. Ben Nasrallah, A. Jemni, Heat and mass transfer models in metal-hydrogen reactor, Int. J. Hydrogen Energy 22 (1) (1997) 67–76.
[3] T. Nakagawa, A. Inomata, H. Aoki, T. Miura, Numerical analysis of heat and mass transfer characteristics in the metal hydride bed, Int. J. Hydrogen Energy 25 (2000) 339–350.
[4] A. Jemni, S. Ben Nasrallah, J. Lamloumi, Experimental and theoretical study of a metal-hydrogen reactor, Int. J. Hydrogen Energy 24 (1999) 631–644.
[5] K. Aldas, M.D. Mat, Y. Kaplan, A three dimensional mathematical model for absorption in a metal hydride bed, Int. J. Hydrogen Energy 27 (2002) 1049–1056.
[6] M.C. Kim, S.Y. Le, J.H. Gu, Numerical prediction of hydrogen storaging performance of finned metal hydride beds, Trans. KSME (B) 22 (4) (1998) 520–529.
[7] Z. Guo, H.J. Sung, Conjugate heat and mass transfer in metal hydride beds in the hydriding process, Int. J. Heat Mass Transfer 42 (1999) 379–382.
[8] I.K. Kim, S. Seung, D.H. Lee, Experiment for the heat and mass transfer in the metal hydride, LG internal report, personal communication, 2002.
[9] S.V. Patamkar, Numerical Heat Transfer and Fluid Flow, Hemisphere, New York, 1980.